



Get Clarity On Generics

Cost-Effective CT & MRI Contrast Agents

**FRESENIUS
KABI**

[WATCH VIDEO](#)

AJNR

This information is current as
of August 21, 2025.

MR Imaging–Based Analysis of Glioblastoma Multiforme: Estimation of *IDH1* Mutation Status






K. Yamashita, A. Hiwatashi, O. Togao, K. Kikuchi, R.
Hatae, K. Yoshimoto, M. Mizoguchi, S.O. Suzuki, T.
Yoshiura and H. Honda

AJNR Am J Neuroradiol 2016, 37 (1) 58-65

doi: <https://doi.org/10.3174/ajnr.A4491>

<http://www.ajnr.org/content/37/1/58>

MR Imaging–Based Analysis of Glioblastoma Multiforme: Estimation of *IDH1* Mutation Status

 K. Yamashita,  A. Hiwatashi,  O. Togao,  K. Kikuchi, R. Hatae, K. Yoshimoto, M. Mizoguchi, S.O. Suzuki, T. Yoshiura, and  H. Honda



ABSTRACT

BACKGROUND AND PURPOSE: Glioblastoma multiforme is highly aggressive and the most common type of primary malignant brain tumor in adults. Imaging biomarkers may provide prognostic information for patients with this condition. Patients with glioma with *isocitrate dehydrogenase 1 (IDH1)* mutations have a better clinical outcome than those without such mutations. Our purpose was to investigate whether the *IDH1* mutation status in glioblastoma multiforme can be predicted by using MR imaging.

MATERIALS AND METHODS: We retrospectively studied 55 patients with glioblastoma multiforme with wild type *IDH1* and 11 patients with mutant *IDH1*. Absolute tumor blood flow and relative tumor blood flow within the enhancing portion of each tumor were measured by using arterial spin-labeling data. In addition, the maximum necrosis area, the percentage of cross-sectional necrosis area inside the enhancing lesions, and the minimum and mean apparent diffusion coefficients were obtained from contrast-enhanced T1-weighted images and diffusion-weighted imaging data. Each of the 6 parameters was compared between patients with wild type *IDH1* and mutant *IDH1* by using the Mann-Whitney *U* test. The performance in discriminating between the 2 entities was evaluated by using receiver operating characteristic analysis.

RESULTS: Absolute tumor blood flow, relative tumor blood flow, necrosis area, and percentage of cross-sectional necrosis area inside the enhancing lesion were significantly higher in patients with wild type *IDH1* than in those with mutant *IDH1* ($P < .05$ each). In contrast, no significant difference was found in the ADC_{minimum} and ADC_{mean} . The area under the curve for absolute tumor blood flow, relative tumor blood flow, percentage of cross-sectional necrosis area inside the enhancing lesion, and necrosis area were 0.850, 0.873, 0.739, and 0.772, respectively.

CONCLUSIONS: Tumor blood flow and necrosis area calculated from MR imaging are useful for predicting the *IDH1* mutation status.

ABBREVIATIONS: ASL = arterial spin-labeling; aTBF = absolute tumor blood flow; AUC = area under the curve; GBM = glioblastoma multiforme; *IDH1* = *isocitrate dehydrogenase 1*; *IDH1m* = mutant *IDH1*; *IDH1w* = wild type *IDH1*; *MGMT* = *O*⁶-methylguanine-DNA methyltransferase; %NEC = percentage of cross-sectional necrosis area inside the enhancing lesion; NEC_{area} = necrosis area; rTBF = relative tumor blood flow; TBF = tumor blood flow

Glioblastoma multiforme (GBM) is highly aggressive and the most common type of primary malignant brain tumor in adults. The characteristic histologic appearance of GBM includes hypercellularity, nuclear polymorphism, high mitotic activity,


prominent microvascular proliferation, and/or necrosis. MR imaging is the main noninvasive technique for diagnosing GBM. Conventional MR imaging techniques including pre- and post-contrast T1WI show precise anatomic localization and/or centrally nonenhancing regions, which are typically related histologically to necrotic areas. Diehn et al¹ provided evidence that the amount of necrosis correlated with outcome in patients with GBM. In addition, correlations were recently identified between the prognosis of patients with GBM and several functional imaging parameters, including ADC derived from DWI, tumor blood volume calculated from DSC, and tumor blood flow (TBF) calculated from arterial spin-labeling (ASL) perfusion MR imaging.^{2–7} ASL is a recently developed MR perfusion imaging technique that has advantages of being noninvasive, not requiring an extrinsic tracer, and allowing reliable absolute quantification, which is not affected by a disrupted blood-brain barrier.⁸ ASL is increasingly

Received March 19, 2015; accepted after revision May 22.

From the Departments of Clinical Radiology (K. Yamashita, A.H., O.T., K.K., T.Y., H.H.), Neurosurgery (R.H., K. Yoshimoto, M.M.), and Neuropathology (S.O.S.), Graduate School of Medical Sciences, Kyushu University, Fukuoka, Japan; and Department of Radiology (T.Y.), Kagoshima University Graduate School of Medical and Dental Sciences, Kagoshima, Japan.

This work was supported by Japan Society for the Promotion of Science KAKENHI (grant No. 26461828).

Please address correspondence to Akio Hiwatashi, MD, PhD, Department of Clinical Radiology, Graduate School of Medical Sciences, Kyushu University, 3-1-1 Maidashi, Higashi-ku, Fukuoka 812-8582, Japan; e-mail: hiwatashi@radiol.med.kyushu-u.ac.jp

 Indicates open access to non-subscribers at www.ajnr.org

<http://dx.doi.org/10.3174/ajnr.A4491>

recognized as a noninvasive method for quantitative CBF measurement for assessing stroke, neurodegenerative diseases, and brain tumors.⁸⁻¹⁴ ADC measurement is a widely used method. Good correlations have been reported between ADC and tumor cellularity, and its utility for application in glioma grading has been addressed in many studies.¹⁵⁻¹⁹

GBMs are classified into primary and secondary GBMs. Primary GBMs develop rapidly de novo, without clinical or histologic evidence of a less malignant precursor lesion.²⁰ In contrast, secondary GBMs develop by progressing from a low-grade diffuse astrocytoma or anaplastic astrocytoma.²⁰ These GBM subtypes are usually indistinguishable histologically. However, genetic evidence suggests that mutations in *isocitrate dehydrogenase (IDH1)* can be used to identify most secondary GBMs. The *IDH1* mutation status is an independent prognostic factor in patients with gliomas.²¹⁻²³ In previous reports, patients with gliomas with *IDH1* mutations had a better clinical outcome (median overall survival = 2.0–3.8 years) than those without such mutations (median overall survival = 0.8–1.1 years).^{24,25} In addition, a specific compound impairs the growth of mutant *IDH1* but not wild type *IDH1* glioma cells.²⁶ These approaches may offer new possibilities for targeted therapy. The status of *O*⁶-methylguanine-DNA methyltransferase (*MGMT*) promotor methylation is also an important factor for the prognosis of patients with GBM. Patients with GBM with *MGMT* promotor methylation are more responsive to temozolomide therapy and have better clinical outcome than those without it.²⁷⁻²⁹ Therefore, the detection of *IDH1* mutations and *MGMT* promotor methylation is of great importance for patients with GBM. Carrillo et al²⁹ suggested that patients with mutant *IDH1* have low vascular endothelial growth factor levels, which are associated with contrast enhancement. These findings led to the hypothesis that measurement of tumor vascularity and the necrosis area would be helpful to differentiate *IDH1* mutation status.

Our purpose was to investigate whether the *IDH1* mutation and *MGMT* methylation status in GBM can be predicted by using MR imaging.

MATERIALS AND METHODS

This study was approved by the institutional review board of Kyushu University Hospital. Informed consent for study participation was waived due to the retrospective nature of this study.

MR imaging data of consecutive patients between May 2007 and August 2013 were obtained and retrospectively analyzed. Considering the effect of perfusion parameters, we excluded enrolled patients who received bevacizumab. Consequently, we examined data for 55 patients with GBM (54 primary and 1 recurrent) with wild type *IDH1* (*IDH1w*: mean age, 54.8 ± 18.6 years; range, 5–83 years) and 11 patients with GBM (5 primary and 6 recurrent) with mutant *IDH1* (*IDH1m*: mean age, 39.9 ± 11.8 years; range, 26–62 years). Among them, ASL was performed in 61.8% (34/55) of patients with *IDH1w* and 81.8% (9/11) of those with *IDH1m*. DWI was performed in 98.1% (54/55) of those with *IDH1w* and 100% (11/11) of those with *IDH1m*, and conventional MR imaging was performed in 100% (55/55) of those with *IDH1w* and 100% (11/11) of those with *IDH1m*. All primary and recurrent GBMs were histopathologically diagnosed by board-

certified neuropathologists. The average interval between MR imaging and the operation was 7.1 days (range, 0–15 days).

MR Imaging

All images were obtained by using a 3T MR imaging unit (Achieva 3T TX; Philips Healthcare, Best, the Netherlands) and an 8-channel head array receiving coil for sensitivity encoding parallel imaging.

ASL

ASL was performed by using quantitative signal targeting with alternating radiofrequency labeling of the arterial region, a pulsed ASL technique developed by Petersen et al.³⁰ The details of the sequence have been described elsewhere.⁷ Our quantitative signal targeting with alternating radiofrequency labeling of the arterial region protocol consisted of 84 dynamic or 42 pairs of labeled and nonlabeled image acquisitions. Of these, 24 pairs were acquired with crusher gradients (velocity-encoding threshold = 4 cm/s) and 12 pairs were acquired without crushers. These 36 pairs were acquired at a flip angle of 35°. An additional 6 pairs were acquired at a lower flip angle (11.7°) without crushers to estimate the actual flip angle that might vary across the brain due to inhomogeneity of B1. Other imaging parameters were as follows: labeling slab thickness = 150 mm, gap between the labeling and imaging slabs = 15 mm, sensitivity encoding factor = 2.5, TR/TE = 4000/22 ms, sampling interval = 300 ms, sampling time points = 13, FOV = 240 mm, matrix size = 64 × 64, imaging time = 5 minutes 52 seconds. Seven 6-mm-thick transverse sections (gap = 2 mm) were placed to cover the tumor.

DWI

DWI was performed by using a single-shot spin-echo echo-planar sequence with the following parameters: TR/TE = 3421/62 ms, 90° flip angle, NEX = 1, 22 transverse sections, sensitivity encoding factor = 2.5, section thickness/gap = 5/1 mm, FOV = 230 mm, 126 × 160 matrix, imaging time = 44.5 seconds. Diffusion sensitizing gradients were applied sequentially in the x, y, and z directions with b factors of 0 and 1000 s/mm².

Conventional MR Imaging

Postcontrast transverse T1-weighted spin-echo images (TR/TE = 400/10 ms, flip angle = 75°, NEX = 1, 22 sections, section thickness/gap = 5/1 mm, FOV = 230 mm, 256 × 173 matrix, imaging time = 2 minutes 43 seconds) were obtained. A standard dose (0.1 mmol/kg body weight) of a gadolinium-based contrast agent, gadopentate dimeglumine (Magnevist; Bayer HealthCare Pharmaceuticals, Wayne, New Jersey), gadoteridol (ProHance; Bracco Diagnostics, Princeton, New Jersey), or gadodiamide (Omniscan; GE Healthcare, Piscataway, New Jersey) was injected intravenously. Precontrast T1-weighted spin-echo, T2-weighted turbo spin-echo, and fluid-attenuated inversion recovery images were also obtained.

Detection of IDH1 Mutations and MGMT Promotor Methylation in Glioblastoma Tissues

GBM samples were obtained from each patient during the operation at our hospital. A portion of the tumor tissue was snap-

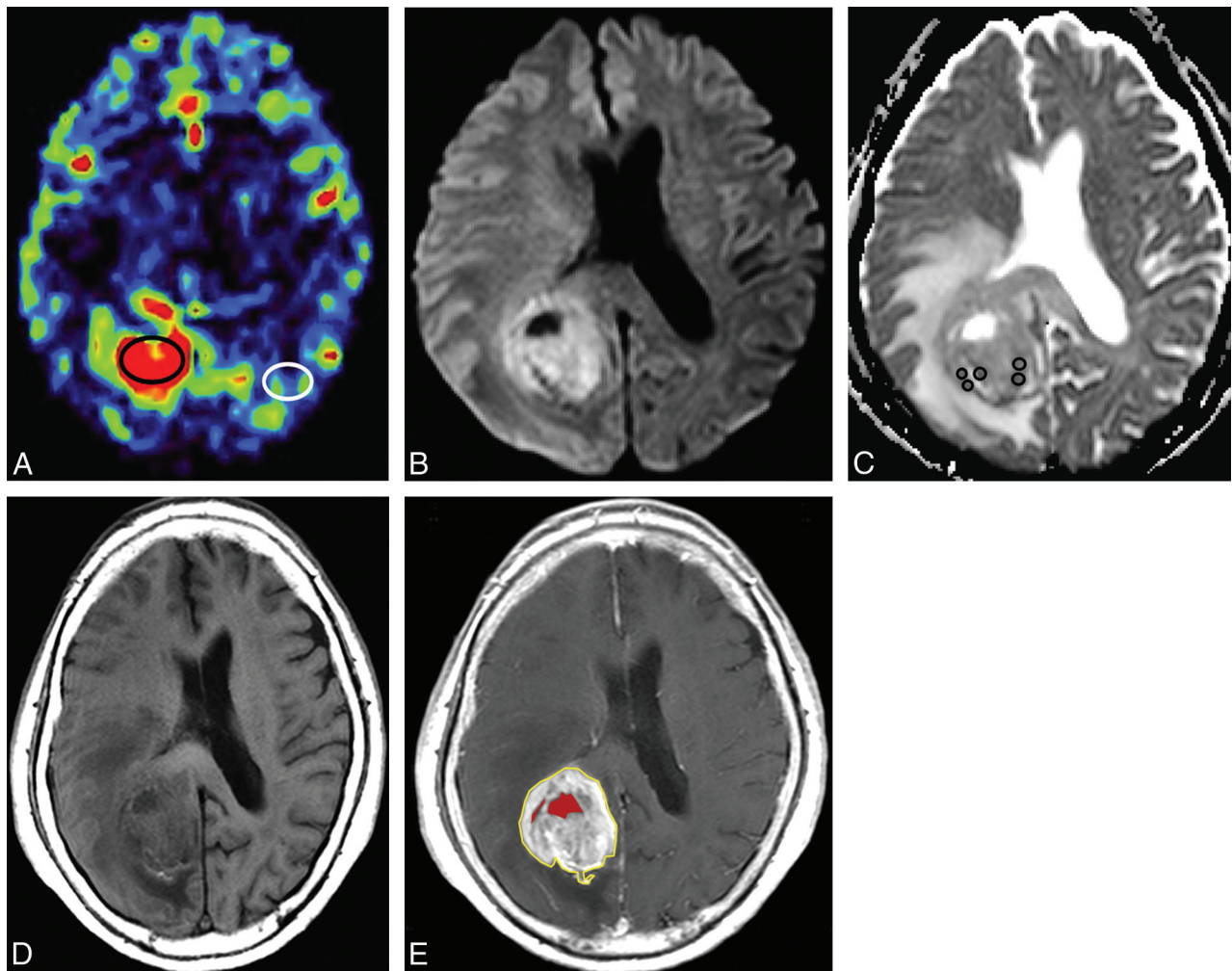


FIG 1. Images showing an example of determination of the TBF (A), ADC (B and C), and necrosis area (D and E). To determine absolute tumor blood flow, we placed the ROI in the enhancing lesion (A, *black circle*). Relative TBF was obtained by normalizing the aTBF by a blood flow measurement from the reference region (*white circle*). For ADC measurements, circular ROIs (C, *black circles*) were placed on ADC maps within the area that corresponded to the enhancing area on postcontrast T1WI, and the mean ADC value was obtained for each ROI. The lowest mean ADC value within all ROIs was determined as the minimum ADC. Regions with relatively low ADC were targeted. D and E, The largest cross-sectional necrosis area (red) and the percentage of the nonenhancing area inside the largest cross-sectional enhancing lesion were identified by manually outlining both the inside (red) and outside (yellow) enhancing contour to determine the NEC_{area} . The enhancing area was carefully determined with reference to both pre- and postcontrast T1WI.

frozen in liquid nitrogen and stored at -80°C . Tumor DNA was isolated from the frozen blocks by using a QIAamp DNA Blood Mini Kit (QIAGEN, Tokyo, Japan). A 129-bp fragment spanning the catalytic domain of *IDH1* including codon 132 was amplified by using the sense primer IDH1f 5'-CGGTCTTCAGAGAAGC-CATT-3' and the antisense primer IDH1r 5'-GCAAAATC-ACATTATTGCCAAC-3', as described previously.^{31,32} Sequences were determined by using an ABI 3100 Genetic Analyzer (Applied Biosystems, Foster City, California).

DNA methylation status of the *MGMT* promoter was determined by bisulfite modification and subsequent methylation-specific polymerase chain reactions. Methylation-specific polymerase chain reactions were performed by using the primers previously reported by Esteller et al³³ and 50-ng bisulfite-modified tumor DNA, in addition to both methylated and unmethylated control samples (CpGenome Universal Methylated and Unmethylated DNA; EMD Millipore, Billerica, Massachusetts). The polymerase chain reaction conditions included 35 cycles of 30

seconds each at 95°C , 60°C , and 72°C . The polymerase chain reaction products were electrophoresed on 3% agarose gels. The method has been described in detail before.³⁴

Image Analysis

The ASL data were analyzed on a desktop computer (Let's note, Panasonic Corporation, Osaka, Japan). Maps of CBF were obtained by using dedicated software running on Interactive Data Language (Research Systems, Boulder, Colorado), which was developed and provided by Petersen et al (National Neuroscience Institute, Singapore). Measurement of blood flow was performed by using ROI analysis by 2 independent neuroradiologists (K. Yamashita and O.T.), who were blinded to the clinical and pathologic information. A free software package (MRlcro, <http://www.mccauslandcenter.sc.edu/mricro/mricro/mricro.html>) was used to draw ROIs on the CBF maps. For each tumor, mean absolute (aTBF) and relative tumor blood flow (rTBF) were measured in each ROI (Fig 1A).³⁵⁻³⁸ Interrater agreement was evaluated by the

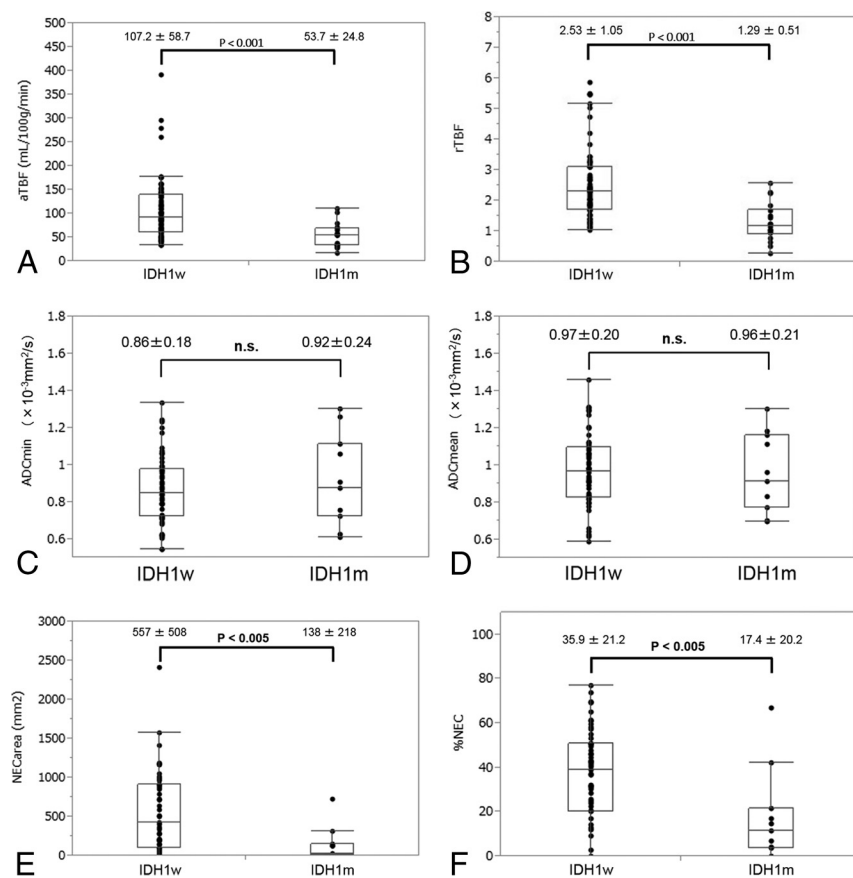


FIG 2. Plots of aTBF (A), rTBF (B), ADC_{minimum} (C), ADC_{mean} (D), NEC_{area} (E), and %NEC (F) in patients with *IDH1w* and *IDH1m*. The aTBF, rTBF, NEC_{area}, and %NEC were significantly higher in patients with *IDH1w* compared with those with *IDH1m* ($P < .05$ each). In contrast, no significant difference was found in the ADC_{minimum} and ADC_{mean}.

Bland-Altman analysis, the intraclass correlation coefficient, and the Spearman rank correlation coefficient.

Maps of ADC were calculated by using the following formula: $\ln(S/S_0) = -b \times \text{ADC}$, where S_0 and S are the signal intensities when the b values are 0 and 1000 s/mm², respectively, and b itself is 1000 s/mm². For ADC measurements, 1 author (K. Yamashita) performed the ROI analysis by using a PACS system. Four or more circular ROIs (area, ≥ 10 mm²) were placed on ADC maps within the area that corresponded to the enhancing area on post-contrast T1WI, and the mean ADC value was obtained for each ROI (Fig 1B, -C).^{4,19,39} Regions with relatively low ADC were targeted, whereas blood vessels, calcifications, necrosis, and hemorrhages were strictly avoided for ROI placement. The lowest and the average mean ADC values within all ROIs were determined as the minimum ADC and the mean ADC.

In addition, the largest cross-sectional necrosis area (NEC_{area}) and the percentage of nonenhancing area inside the largest cross-sectional enhancing lesion (%NEC) were identified by manually outlining both the inside and outside enhancing contour to determine the necrosis area. The enhancing area was carefully determined with reference to both pre- and postcontrast T1WI (Fig 1D, -E). These determinations were performed by 1 author (K. Yamashita), followed by visual inspection by another neuroradiologist (O.T.). When multifocal lesions were noted, the maximum enhancing lesion was targeted.

Each of the 6 parameters (aTBF, rTBF, ADC_{minimum}, ADC_{mean}, NEC_{area}, and %NEC) was compared between patients with *IDH1w* and *IDH1m* and between patients with a methylated *MGMT* promoter and those with an unmethylated *MGMT* promoter by using the Student t test. A P value $< .05$ was statistically significant. The performance in discriminating between patients with *IDH1w* and *IDH1m* was evaluated by using receiver operating characteristic analysis. Area under the curve (AUC) values for the discrimination were calculated for parameters that were statistically significant. Multivariate logistic regression analysis was performed to evaluate the combination of the parameters. AUC values were compared with each other by using a non-parametric approach.⁴⁰ All statistical analyses were performed by using JMP 11 Pro software (SAS Institute, Cary, North Carolina).

RESULTS

aTBF, rTBF, NEC_{area}, and %NEC were significantly higher in patients with *IDH1w* (mean aTBF = 107.2 ± 58.7 mL/100 g/min, mean rTBF = 2.53 ± 1.05, mean NEC_{area} = 557 ± 508 mm², and mean %NEC = 35.9% ± 21.2%)

than in those with *IDH1m* (mean aTBF = 53.7 ± 24.8 mL/100 g/min, mean rTBF = 1.29 ± 0.51, mean NEC_{area} = 138 ± 218 mm², and mean %NEC = 17.4% ± 20.2%) ($P < .05$ each, Fig 2). In contrast, no significant differences were found in ADC_{minimum} (ADC_{minimum} = 0.86 ± 0.18 × 10⁻³ mm²/s; range, 0.54–1.33 × 10⁻³ mm²/s in *IDH1w*, 0.92 ± 0.24 × 10⁻³ mm²/s; range, 0.61–1.30 × 10⁻³ mm²/s in *IDH1m*) and ADC_{mean} (ADC_{mean} = 0.97 ± 0.20 × 10⁻³ mm²/s; range, 0.59–1.46 × 10⁻³ mm²/s in *IDH1w*, 0.96 ± 0.21 × 10⁻³ mm²/s; range, 0.69–1.30 × 10⁻³ mm²/s in *IDH1m*) ($P > .05$ each).

No significant differences were observed in any parameters between patients with a methylated *MGMT* promoter and those with an unmethylated *MGMT* promoter (Table).

The optimal cutoff value was 70.0 mL/100 g/min for aTBF with 76.5% sensitivity, 88.9% specificity, and 79.1% accuracy. For rTBF, the optimal cutoff value was 1.55 with 88.2% sensitivity, 77.8% specificity, and 86.0% accuracy. For %NEC, the optimal cutoff value was 22.5 with 72.7% sensitivity, 81.8% specificity, and 74.2% accuracy. For NEC_{area}, the optimal cutoff value was 151 mm² with 72.7% sensitivity, 81.8% specificity, and 74.2% accuracy. The AUCs for aTBF, rTBF, %NEC, and NEC_{area} were 0.850, 0.873, 0.739, and 0.772, respectively (Fig 3). No significant difference in AUC values was found among aTBF, rTBF, %NEC, and NEC_{area}. The combination of the 4 parameters increased the diagnostic performance (AUC = 0.915). The AUC value was sig-

Comparison between 6 parameters and MGMT methylation status

	Methylated	Unmethylated	P Value
aTBF (mL/100 g/min)	100.4 ± 1.13 (n = 19)	99.4 ± 55.4 (n = 15)	.96
rTBF	2.54 ± 1.31 (n = 19)	2.35 ± 0.81 (n = 15)	.62
ADC _{minimum} (×10 ³ mm ² /s)	0.88 ± 0.19 (n = 24)	0.84 ± 0.20 (n = 21)	.57
ADC _{mean} (×10 ³ mm ² /s)	0.97 ± 0.19 (n = 24)	0.96 ± 0.21 (n = 21)	.92
NEC _{area} (mm ²)	503 ± 424 (n = 25)	621 ± 430 (n = 21)	.36
%NEC	37.3 ± 21.1 (n = 25)	38.6 ± 22.7 (n = 21)	.85

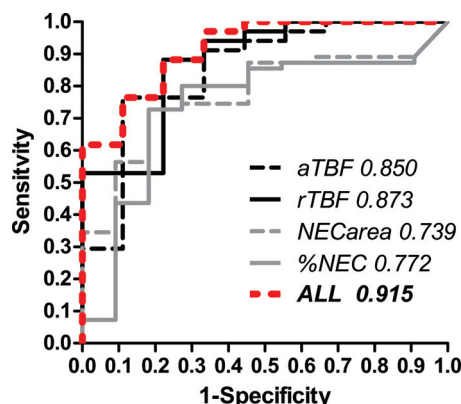


FIG 3. Receiver operating characteristic curves for discrimination between patients with *IDH1w* and those with *IDH1m* with the parameters aTBF, rTBF, NEC_{area}, and %NEC. The AUC was significantly higher with the combination of all parameters than with NEC_{area} or %NEC alone ($P < .05$).

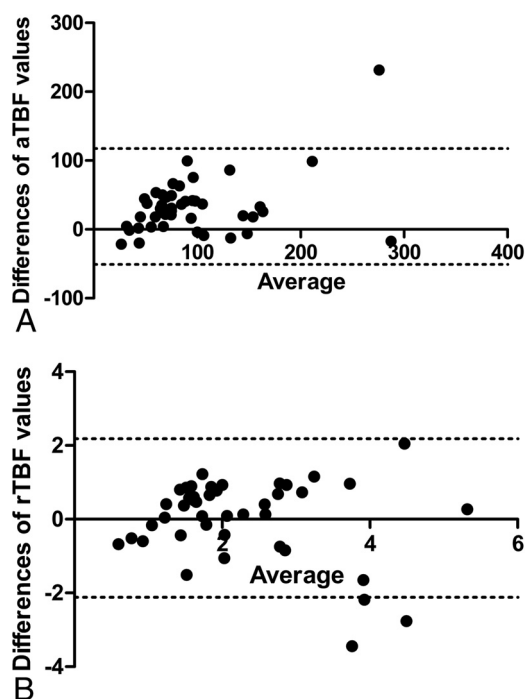


FIG 4. Bland-Altman plots showing the interobserver variability of the differences versus average of aTBF (A) and rTBF (B) values. Dashed lines represent the 95% limits of agreement.

nificantly higher with the combination of all parameters than with NEC_{area} or %NEC alone ($P < .05$).

Bland-Altman analysis resulted in a mean bias of 33.4 with 95% limits of agreement in differences versus the average of the aTBF values, which ranged from -50.7 to 117.6 , and 0.03 with

95% limits of agreement in differences versus the average of the rTBF values, which ranged from -2.12 to 2.18 (Fig 4). The intraclass correlation coefficient was 0.861 (95% confidence interval, 0.743 – 0.925) for aTBF and 0.745 (95% confidence interval, 0.530 – 0.862) for rTBF, which indicated a high correlation. For the Spearman rank correlation

coefficient, good correlation was shown for both aTBF ($\rho = 0.774$, $P < .01$) and rTBF ($\rho = 0.709$, $P < .01$) for the values between the 2 neuroradiologists.

Figures 5 and 6 show representative cases of *IDH1w* and *IDH1m*, respectively.

DISCUSSION

Our study demonstrated that both aTBF and rTBF were significantly higher in patients with *IDH1w* than in those with *IDH1m*. Microvascular proliferation is induced by the vascular endothelial growth factor, which shows markedly higher expression in primary than secondary GBMs.⁴¹ Diehn et al¹ suggested that vascular endothelial growth factor production is associated with angiogenesis and contrast enhancement. The relationship between vascular endothelial growth factor and *IDH1* remains uncertain. However, these results suggested that a correlation may exist between tumor vascularity and *IDH1* mutation status. In addition, a previous study by using ASL showed that high TBF in GBM is associated with poor overall survival.⁴² ASL measurements may provide additional prognostic information.

In this study, both NEC_{area} and %NEC were significantly higher in patients with *IDH1w* than in those with *IDH1m*. In GBM, hypoxia-mediated activation of the coagulation system causes intravascular thrombosis, which further increases intratumoral hypoxia and leads to abnormal endothelial cell proliferation and tumor necrosis.⁴³ Previous studies demonstrated that large areas of ischemic and/or pseudopalisading necrosis are more frequent in primary than in secondary GBMs,⁴⁴ and in patients with *IDH1w* than in those with *IDH1m*.²⁵ Carlson et al⁴⁵ indicated that necrosis is associated with higher levels of vascular endothelial growth factor. Our results are in line with these previous reports.

We found that both TBF and the necrosis area in patients with *IDH1w* were significantly higher than in those with *IDH1m*. The AUC value was significantly higher with the combination of all 4 parameters (aTBF, rTBF, NEC_{area}, and %NEC) than with NEC_{area} or %NEC alone. This is the first report to compare the performance of ASL, DWI, and gadolinium T1WI for predicting the *IDH1* mutation status in GBM, to our knowledge. Our results suggested that the combination of TBF derived from ASL and measurement of the necrosis area may be a surrogate marker for predicting the *IDH1* mutation status. Noninvasive estimates of tumor vascularity (aTBF, rTBF) and necrosis (NEC_{area}, %NEC) may be useful for evaluating the prognosis of patients with GBM and their *IDH1* mutation status. Patients with *IDH1w* and *IDH1m* follow different clinical courses, and GBMs with these mutations are considered to be 2 distinct disease entities.⁴⁶ TBF and tumor necrosis area measurements play supportive roles as predictors of

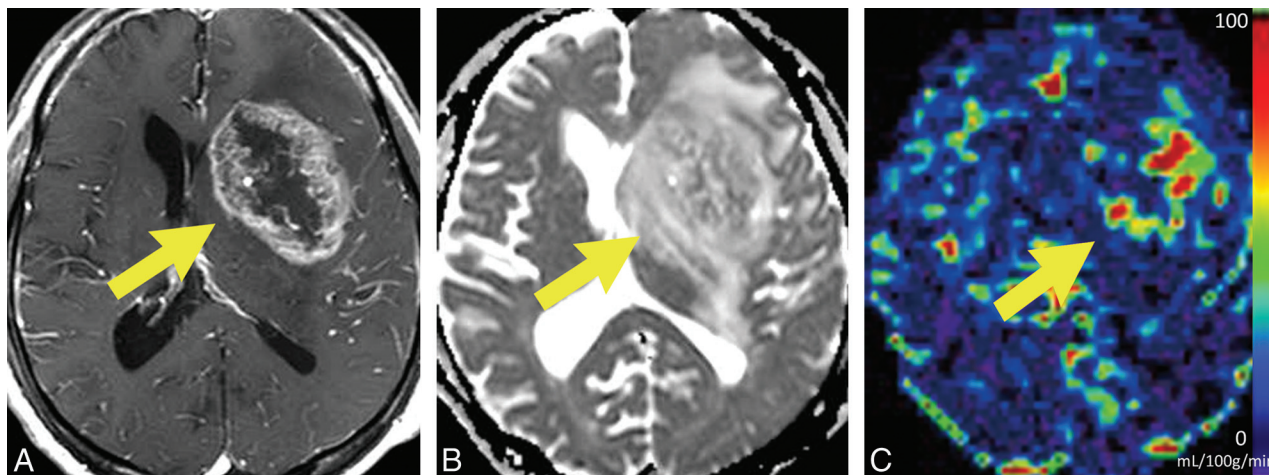


FIG 5. Contrast-enhanced T1WI (A), ADC map derived from DWI (B), and TBF map derived from ASL (C) of a 73-year-old woman with *IDH1w*. High aTBF (96.2 mL/100 g/min) and rTBF (2.78) were demonstrated in the enhancing tumor. The tumor also showed a high NEC_{area} (518 mm²) and %NEC (44.2).

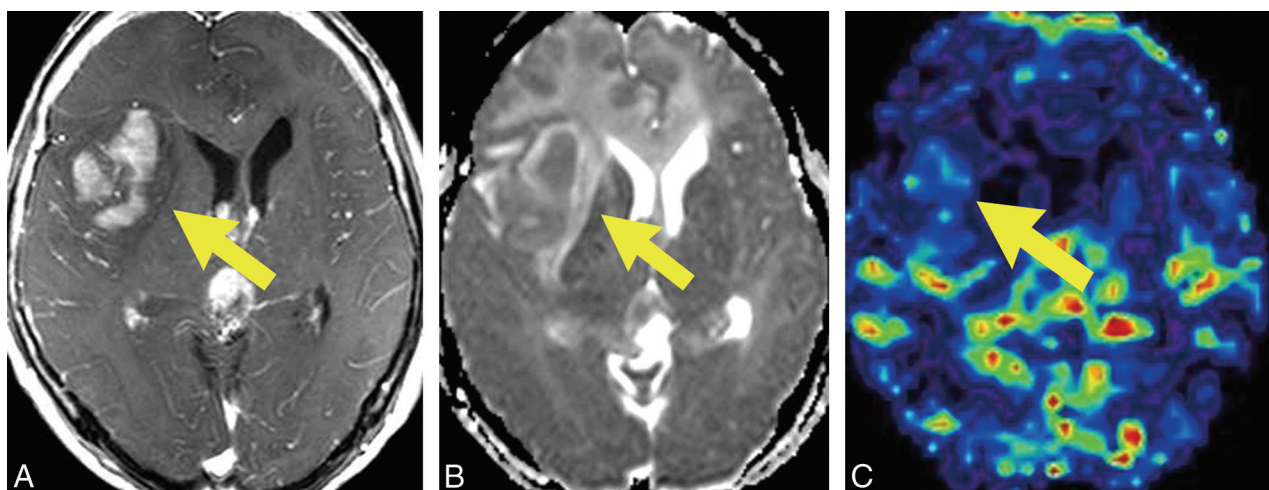


FIG 6. Contrast-enhanced T1WI (A), ADC map derived from DWI (B), and TBF map derived from ASL (C) of a 62-year-old woman with *IDH1m*. ASL perfusion demonstrated a relatively low aTBF (31.6 mL/100 g/min) and rTBF (1.05) in the enhancing tumor. The tumor also showed a low NEC_{area} (30 mm²) and %NEC (4.14).

the response to current treatment and tumor aggressiveness. These measurements may provide important information for selecting more or less intensive treatment.

With ADC measurement, no significant difference was found between patients with *IDH1w* and those with *IDH1m* in our study. Lee et al⁴⁷ showed that the mean ADC value in patients with *IDH1m* was significantly higher than that in those with *IDH1w*. This difference may be attributed to patient selection. The *IDH1m* group had a significantly higher proportion of anaplastic astrocytoma than the *IDH1w* group in their study. In our study, only patients with GBM were included. Lazovic et al⁴⁸ found no significant differences in ADC in nonnecrotic tumor regions between patients with *IDH1w* and those with *IDH1m*. On the basis of a radiologic-pathologic correlation study, no significant correlation between the Ki-67 labeling index and minimum ADC was noted for the GBM group.¹⁹ Our results are consistent with those in the literature.

IDH1m and *MGMT* promotor methylation are related to a better clinical prognosis.^{21–23,27–29} A selective inhibitor of mutant

IDH1 has been proved to delay glioma growth.²⁶ Patients with GBM with *MGMT* promotor methylation are more sensitive to temozolomide therapy and are associated with a favorable outcome.^{27–29} Noninvasive prediction of *IDH1* mutation and *MGMT* promotor methylation could contribute to the development of treatment strategies such as further targeted therapy. No significant differences were observed in any parameters derived from MR imaging between patients with a methylated *MGMT* promotor and those with an unmethylated *MGMT* promotor. Carrillo et al²⁹ indicated that the methylation status does not correlate with any imaging features (size, enhancement, noncontrast enhancing tumor, necrosis, edema, cysts, and location). The group of patients with an unmethylated *MGMT* promotor showed a significant difference in mean rCBV between pseudoprogression and real progression, though the group with a methylated *MGMT* promotor showed no significant difference in another study.⁴⁹ These results suggest that predicting *MGMT* promotor methylation status from MR imaging may be challenging.²⁹

Our study has some limitations. First, as mentioned earlier, not all patients were studied with all 3 imaging modalities (ASL, DWI, and postcontrast T1WI). Some recurrent cases of *IDH1w* and *IDH1m* were included in our study. The tumor sample was not acquired stereotactically before resection. However, a 3D MR image overlay navigation system and 5-aminolevulinic acid fluorescence-guided surgery were used to avoid necrotic or nonenhancing tumor regions when obtaining the GBM sample. Finally, automated MR imaging volumetric quantification of tumor necrosis was not applied because we believe that both pre- and post-contrast T1WI are required to correctly determine the enhancing area.

CONCLUSIONS

Our results suggested that TBF calculated from ASL and tumor necrosis area derived from conventional MR imaging are useful for predicting the *IDH1* mutation status.

Disclosures: Koji Yamashita—RELATED: Grant: Japan Society for the Promotion of Science (Japanese grant) KAKENHI 26461828.* Akio Hiwatashi—UNRELATED: Grants/Grants Pending: Japan Society for the Promotion of Science KAKENHI for MRI. *Money paid to the institution.

REFERENCES

- Diehn M, Nardini C, Wang DS, et al. Identification of noninvasive imaging surrogates for brain tumor gene-expression modules. *Proc Natl Acad Sci U S A* 2008;105:5213–18 CrossRef Medline
- Henson JW, Gaviani P, Gonzalez RG. MRI in treatment of adult gliomas. *Lancet Oncol* 2005;6:167–75 CrossRef Medline
- Hakyemez B, Erdogan C, Bolca N, et al. Evaluation of different cerebral mass lesions by perfusion-weighted MR imaging. *J Magn Reson Imaging* 2006;24:817–24 CrossRef Medline
- Calli C, Kitis O, Yuntan N, et al. Perfusion and diffusion MR imaging in enhancing malignant cerebral tumors. *Eur J Radiol* 2006;58:394–403 CrossRef Medline
- Yamasaki F, Kurisu K, Satoh K, et al. Apparent diffusion coefficient of human brain tumors at MR imaging. *Radiology* 2005;235:985–91 CrossRef Medline
- Weber MA, Zoubaa S, Schlieter M, et al. Diagnostic performance of spectroscopic and perfusion MRI for distinction of brain tumors. *Neurology* 2006;66:1899–906 CrossRef Medline
- Yamashita K, Yoshiura T, Hiwatashi A, et al. Differentiating primary CNS lymphoma from glioblastoma multiforme: assessment using arterial spin labeling, diffusion-weighted imaging, and ¹⁸F-fluorodeoxyglucose positron emission tomography. *Neuroradiology* 2013;55:135–43 CrossRef Medline
- Warmuth C, Gunther M, Zimmer C. Quantification of blood flow in brain tumors: comparison of arterial spin labeling and dynamic susceptibility-weighted contrast-enhanced MR imaging. *Radiology* 2003;228:523–32 CrossRef Medline
- Alsop DC, Detre JA, Grossman M. Assessment of cerebral blood flow in Alzheimer's disease by spin-labeled magnetic resonance imaging. *Ann Neurol* 2000;47:93–100 CrossRef Medline
- Chalela JA, Alsop DC, Gonzalez-Atavales JB, et al. Magnetic resonance perfusion imaging in acute ischemic stroke using continuous arterial spin labeling. *Stroke* 2000;31:680–87 CrossRef Medline
- Detre JA, Alsop DC, Vives LR, et al. Noninvasive MRI evaluation of cerebral blood flow in cerebrovascular disease. *Neurology* 1998;50:633–41 CrossRef Medline
- Noguchi T, Yoshiura T, Hiwatashi A, et al. Perfusion imaging of brain tumors using arterial spin-labeling: correlation with histopathologic vascular density. *AJNR Am J Neuroradiol* 2008;29:688–93 CrossRef Medline
- Yoshiura T, Hiwatashi A, Noguchi T, et al. Arterial spin labelling at 3-T MR imaging for detection of individuals with Alzheimer's disease. *Eur Radiol* 2009;19:2819–25 CrossRef Medline
- Tourdias T, Rodrigo S, Oppenheim C, et al. Pulsed arterial spin labeling applications in brain tumors: practical review. *J Neuroradiol* 2008;35:79–89 CrossRef Medline
- Kim HS, Kim SY. A prospective study on the added value of pulsed arterial spin-labeling and apparent diffusion coefficients in the grading of gliomas. *AJNR Am J Neuroradiol* 2007;28:1693–99 CrossRef Medline
- Kono K, Inoue Y, Nakayama K, et al. The role of diffusion-weighted imaging in patients with brain tumors. *AJNR Am J Neuroradiol* 2001;22:1081–88 Medline
- Provenzale JM, Mukundan S, Barboriak DP. Diffusion-weighted and perfusion MR imaging for brain tumor characterization and assessment of treatment response. *Radiology* 2006;239:632–49 CrossRef Medline
- Tien RD, Felsberg GJ, Friedman H, et al. MR imaging of high-grade cerebral gliomas: value of diffusion-weighted echoplanar pulse sequences. *AJR Am J Roentgenol* 1994;162:671–77 CrossRef Medline
- Higano S, Yun X, Kumabe T, et al. Malignant astrocytic tumors: clinical importance of apparent diffusion coefficient in prediction of grade and prognosis. *Radiology* 2006;241:839–46 CrossRef Medline
- Ohgaki H, Kleihues P. Genetic pathways to primary and secondary glioblastoma. *Am J Pathol* 2007;170:1445–53 CrossRef Medline
- Ichimura K, Pearson DM, Kocalkowski S, et al. IDH1 mutations are present in the majority of common adult gliomas but rare in primary glioblastomas. *Neuro Oncol* 2009;11:341–47 CrossRef Medline
- Myung JK, Cho HJ, Park CK, et al. IDH1 mutation of gliomas with long-term survival analysis. *Oncol Rep* 2012;28:1639–44 Medline
- Ducray F, Marie Y, Sanson M. IDH1 and IDH2 mutations in glioma. *N Engl J Med* 2009;360:2248–49; author reply 2249 Medline
- Parsons DW, Jones S, Zhang X, et al. An integrated genomic analysis of human glioblastoma multiforme. *Science* 2008;321:1807–12 CrossRef Medline
- Nobusawa S, Watanabe T, Kleihues P, et al. IDH1 mutations as molecular signature and predictive factor of secondary glioblastomas. *Clin Cancer Res* 2009;15:6002–07 CrossRef Medline
- Rohle D, Popovici-Muller J, Palaskas N, et al. An inhibitor of mutant IDH1 delays growth and promotes differentiation of glioma cells. *Science* 2013;340:626–30 CrossRef Medline
- Kreth S, Thon N, Eigenbrod S, et al. O-methylguanine-DNA methyltransferase (MGMT) mRNA expression predicts outcome in malignant glioma independent of MGMT promoter methylation. *PLoS One* 2011;6:e17156 CrossRef Medline
- Hegi ME, Liu L, Herman JG, et al. Correlation of O6-methylguanine methyltransferase (MGMT) promoter methylation with clinical outcomes in glioblastoma and clinical strategies to modulate MGMT activity. *J Clin Oncol* 2008;26:4189–99 CrossRef Medline
- Carrillo JA, Lai A, Nghiemphu PL, et al. Relationship between tumor enhancement, edema, IDH1 mutational status, MGMT promoter methylation, and survival in glioblastoma. *AJNR Am J Neuroradiol* 2012;33:1349–55 CrossRef Medline
- Petersen ET, Lim T, Golay X. Model-free arterial spin labeling quantification approach for perfusion MRI. *Magn Reson Med* 2006;55:219–32 CrossRef Medline
- Ma X, Yoshimoto K, Guan Y, et al. Associations between microRNA expression and mesenchymal marker gene expression in glioblastoma. *Neuro Oncol* 2012;14:1153–62 CrossRef Medline
- Fuller GN, Hess KR, Rhee CH, et al. Molecular classification of human diffuse gliomas by multidimensional scaling analysis of gene expression profiles parallels morphology-based classification, correlates with survival, and reveals clinically-relevant novel glioma subsets. *Brain Pathol* 2002;12:108–16 CrossRef Medline
- Esteller M, Garcia-Foncillas J, Andion E, et al. Inactivation of the DNA-repair gene MGMT and the clinical response of gliomas to alkylating agents. *N Engl J Med* 2000;343:1350–54 CrossRef Medline
- Araki Y, Mizoguchi M, Yoshimoto K, et al. Quantitative digital as-

- assessment of MGMT immunohistochemical expression in glioblastoma tissue. *Brain Tumor Pathol* 2011;28:25–31 [CrossRef Medline](#)
35. Yamashita K, Yoshiura T, Hiwatashi A, et al. Arterial spin labeling of hemangioblastoma: differentiation from metastatic brain tumors based on quantitative blood flow measurement. *Neuroradiology* 2012;54:809–13 [CrossRef Medline](#)
36. Lehmann P, Monet P, de Marco G, et al. A comparative study of perfusion measurement in brain tumours at 3 Tesla MR: arterial spin labeling versus dynamic susceptibility contrast-enhanced MRI. *Eur Neurol* 2010;64:21–26 [CrossRef Medline](#)
37. Löbel U, Sedlacik J, Reddick WE, et al. Quantitative diffusion-weighted and dynamic susceptibility-weighted contrast-enhanced perfusion MR imaging analysis of T2 hypointense lesion components in pediatric diffuse intrinsic pontine glioma. *AJNR Am J Neuroradiol* 2011;32:315–22 [CrossRef Medline](#)
38. Loeber RT, Sherwood AR, Renshaw PF, et al. Differences in cerebellar blood volume in schizophrenia and bipolar disorder. *Schizophr Res* 1999;37:81–89 [CrossRef Medline](#)
39. Sugahara T, Korogi Y, Kochi M, et al. Usefulness of diffusion-weighted MRI with echo-planar technique in the evaluation of cellularity in gliomas. *J Magn Reson Imaging* 1999;9:53–60 [Medline](#)
40. DeLong ER, DeLong DM, Clarke-Pearson DL. Comparing the areas under two or more correlated receiver operating characteristic curves: a nonparametric approach. *Biometrics* 1988;44:837–45 [CrossRef Medline](#)
41. Godard S, Getz G, Delorenzi M, et al. Classification of human astrocytic gliomas on the basis of gene expression: a correlated group of genes with angiogenic activity emerges as a strong predictor of subtypes. *Cancer Res* 2003;63:6613–25 [Medline](#)
42. Farace P, Amelio D, Ricciardi GK, et al. Early MRI changes in glioblastoma in the period between surgery and adjuvant therapy. *J Neurooncol* 2013;111:177–85 [CrossRef Medline](#)
43. Ohgaki H, Kleihues P. The definition of primary and secondary glioblastoma. *Clin Cancer Res* 2013;19:764–72 [CrossRef Medline](#)
44. Homma T, Fukushima T, Vaccarella S, et al. Correlation among pathology, genotype, and patient outcomes in glioblastoma. *J Neuropathol Exp Neurol* 2006;65:846–54 [CrossRef Medline](#)
45. Carlson MR, Pope WB, Horvath S, et al. Relationship between survival and edema in malignant gliomas: role of vascular endothelial growth factor and neuronal pentraxin 2. *Clin Cancer Res* 2007;13:2592–98 [CrossRef Medline](#)
46. Lai A, Kharbanda S, Pope WB, et al. Evidence for sequenced molecular evolution of IDH1 mutant glioblastoma from a distinct cell of origin. *J Clin Oncol* 2011;29:4482–90 [CrossRef Medline](#)
47. Lee S, Choi SH, Ryoo I, et al. Evaluation of the microenvironmental heterogeneity in high-grade gliomas with IDH1/2 gene mutation using histogram analysis of diffusion-weighted imaging and dynamic-susceptibility contrast perfusion imaging. *J Neurooncol* 2015;121:141–50 [CrossRef Medline](#)
48. Lazovic J, Soto H, Piccioni D, et al. Detection of 2-hydroxyglutaric acid in vivo by proton magnetic resonance spectroscopy in U87 glioma cells overexpressing isocitrate dehydrogenase-1 mutation. *Neuro Oncol* 2012;14:1465–72 [CrossRef Medline](#)
49. Kong DS, Kim ST, Kim EH, et al. Diagnostic dilemma of pseudoprogression in the treatment of newly diagnosed glioblastomas: the role of assessing relative cerebral blood flow volume and oxygen-6-methylguanine-DNA methyltransferase promoter methylation status. *AJNR Am J Neuroradiol* 2011;32:382–87 [CrossRef Medline](#)